

Direct Photon Results from CDF

Tingjun Yang^{1,a} for the CDF Collaboration

¹Fermilab, Batavia, IL, USA

Abstract. Direct (prompt) photon production is a field of very high interest in hadron colliders. It provides probes to search for new phenomena and to test QCD predictions. In this article, two recent cross-section results for direct photon production using the full CDF Run II data set are presented: diphoton production and photon production in association with a heavy quark.

1 Introduction

Direct photon (γ) production in hadron colliders provides a clean probe to test quantum chromodynamics (QCD) predictions. A better understanding of such processes can improve the background modeling in the searches for new physics with photon final state. In this article, two recent cross-section results for direct photon production in $p\bar{p}$ collisions at $\sqrt{s} = 1.96$ TeV are presented: diphoton production [1] and photon production in association with a heavy quark Q (b or c) [2]. Both results use the full data set collected by the CDF II detector.

The CDF II detector [3] has a cylindrical geometry with approximate forward-backward and azimuthal symmetry. It contains a tracking system consisting of silicon microstrip detectors and a cylindrical open-cell drift chamber immersed in a 1.4 T magnetic field parallel to the beam axis. The silicon subsystem is used for reconstructing charged-particle trajectories (tracks) and heavy-flavor-decay vertices displaced from the primary interaction point. Electromagnetic (EM) and hadronic calorimeters surrounding the tracking system with pointing-tower geometry are used to measure photon energies. At a depth approximately corresponding to the maximum development of the EM shower, the EM calorimeters contain fine-grained detectors (central electromagnetic strip chambers) that measure the shower profile. Drift chambers and scintillators located outside the calorimeters identify muons.

2 Cross Section for Direct Diphoton Production

Precise measurements of the production cross sections for diphotons are important for the searches for new phenomena, such as extra spatial dimensions, and for improvements in the precision of the measurements of the production cross section and the decay branching ratio of the Higgs boson into a photon pair. Diphoton production is

also used to test QCD both in the perturbative scheme (pQCD) and in nonperturbative schemes, such as soft-gluon resummation methods and photons from quark fragmentation. This article presents the final diphoton measurements from CDF using the full data set collected in 2001-2011 corresponding to a total integrated luminosity of 9.5 fb^{-1} .

Inclusive diphoton events are selected online by requiring two isolated electromagnetic clusters with $E_T > 12$ GeV each or two electromagnetic clusters with $E_T > 18$ GeV and no isolation requirement. In the offline analysis additional requirements are imposed to identify a sample rich in prompt photons. The pseudorapidity of each photon in the event is restricted to the region $|\eta| < 1$. The photon transverse energy is required to exceed 17 GeV for the first photon and 15 GeV for the second photon. The transverse energy measured by the calorimeter in an isolation cone with a radius in $\eta - \phi$ space of 0.4 around each photon is required not to exceed 2 GeV.

The background from events where one or both reconstructed photons are misidentified jets is subtracted with a 4×4 matrix technique using the track isolation as the discriminant between the signal and background [4]. The differential cross section for diphoton production is obtained from the histogram of the estimated signal yield as a function of each relevant kinematic variable. The average cross section in a bin is determined by dividing the yield by the product of the trigger efficiency, the selection efficiency and acceptance, the integrated luminosity, and the bin size.

The experimental results are compared with six theoretical calculations: (i) the fixed NLO predictions of the DIPHOX program, including nonperturbative parton fragmentation into photons at NLO, (ii) the predictions of the RESBOS program where the cross section is accurate to NLO, but also has an analytical initial-state soft-gluon resummation, (iii) the predictions of the PYTHIA parton-shower program including photons radiated from initial- and final-state quarks, (iv) the fixed NLO predictions of the MCFM program, including nonperturbative parton frag-

^ae-mail: tjiang@fnal.gov

mentation into photons at LO, (v) the fixed next-to-next-to-leading order (NNLO) predictions of a recent calculation, and (vi) the predictions of the SHERPA program, based on a matrix element calculation merged with the parton shower model.

The measured cross section for diphoton production integrated over the acceptance is $12.3 \pm 0.2_{\text{stat}} \pm 3.5_{\text{sys}}$ pb. The predictions for the integrated cross section are 10.6 ± 0.6 pb from DIPHOX, 11.3 ± 2.4 pb from RESBOS, 9.2 pb from PYTHIA, 12.4 ± 4.4 pb from SHERPA, 11.5 ± 0.3 pb from MCFM, and $11.8^{+1.7}_{-0.6}$ pb from the NNLO calculation. The SHERPA scale uncertainty is large because it also accounts for parton shower. The PYTHIA uncertainty is unreported. All predictions are consistent with the measurement.

Figure 1 shows the comparisons between the observed and predicted distributions in diphoton mass M , transverse momentum P_T of the photon pair, and azimuthal separation $\Delta\phi$ between the momenta of the two photons in the event. All predictions for the mass distribution show a reasonable agreement with the data for all calculations above the maximum at $30 \text{ GeV}/c^2$ except the PYTHIA $\gamma\gamma$ calculation. All predictions underestimate the data rate around and below the maximum. In the P_T spectrum, the PYTHIA, DIPHOX, RESBOS and MCFM predictions underestimate the data in the region between 30 and 60 GeV/c , where the contribution from quark fragmentation is important. Both NNLO and SHERPA predictions describe the data fairly well in this region. For $P_T < 20 \text{ GeV}/c$, where soft-gluon radiation becomes important, the RESBOS, PYTHIA and SHERPA predictions provide a good description of the data because of the resummation of multiple soft-gluon emission amplitudes through either analytical calculation or parton showering. The fixed-order predictions diverge in the limit of vanishing P_T . The RESBOS, PYTHIA and SHERPA predictions show a good agreement with the data at larger $\Delta\phi$, where the diphoton system acquires substantial transverse momentum due to multiple soft-gluon emission. The NNLO calculation is the only prediction consistent with the data in the low $\Delta\phi$ tail, which contains photon pairs with very low mass and relatively high P_T .

3 Cross Section for Direct Photon Production in Association with a Heavy Quark

The cross section for direct photon production in association with a heavy quark in hadronic collisions provides valuable information on the probability distributions of partons inside the initial-state hadrons. At photon transverse energy E_T^γ smaller than 100 GeV, such events are produced predominantly by the Compton scattering process, while at higher energies the dominant process is quark-antiquark annihilation with gluon (g) splitting to heavy quarks. It is conventional to assume that the charm (c) and bottom (b) quarks in the proton arise only from gluon splitting. However, there are other models that allow the existence of intrinsic heavy quarks in the proton. A cross-section measurement of $\gamma + Q + X$ (X can be any final-state particle) production provides information

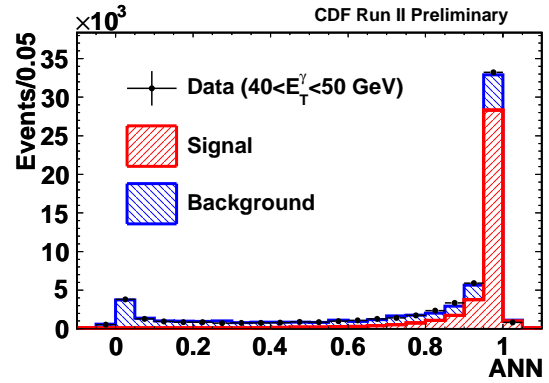


Figure 2. The fit to the ANN distribution for photon candidates with E_T^γ between 40 and 50 GeV. The points are data, and the stacked, shaded histograms represent the estimated contributions from the fit of the prompt photon signal and false photon background.

on the heavy-quark and gluon parton distribution functions (PDFs) and on the rate of final-state gluon splitting to heavy quarks. This article presents the final CDF measurements of the cross sections for photon with heavy-flavor jets, using the full data set from 9.1 fb^{-1} of integrated luminosity, exploring E_T^γ up to 300 GeV.

The photo-plus-heavy-jet events are selected online by requiring at least one energy cluster consistent with a photon in the final state. The offline event selection required each event to have at least one photon candidate that has pseudorapidity in the fiducial region of the central calorimeter ($|\eta| < 1$). Photon candidates are required to have $E_T^\gamma > 30 \text{ GeV}$. An artificial neural network (ANN) is constructed to reduce background. At least one jet must be present in each event. Jets are reconstructed using the JETCLU algorithm with a cone radius 0.4. We select jets that have $E_T > 20 \text{ GeV}$ and $|\eta| < 1.5$. At least one jet is required to be classified as a heavy-flavor jet using a secondary-vertex tagger. The selected jet is required to be reconstructed in a volume outside a cone with a radius in $\eta - \phi$ space of 0.4 surrounding the photon candidate.

There are two main background sources: jets misidentified as photons (false photons) and light-flavor jets mimicking heavy-flavor jets. To estimate the rate of false photons, the photon ANN distribution in data is fitted to a linear combination of templates for photons and jets, obtained from simulated samples. A fit is performed in each E_T^γ interval to get the prompt photon fractions (purities). One example fit is shown in Figure 2.

Backgrounds to heavy-flavor jets arise from light-flavor jets where random combinations of tracks mimic a displaced vertex. The fractions of b - and c -jets are determined by fitting the invariant mass (M_{SecVtx}) of the system of charged particles, assumed to be pions, originating at the secondary vertex, using the templates for b -, c -, and light-quark jets constructed with a simulated sample. The contribution to the M_{SecVtx} distribution from events with a false photon is modeled using dijet data. Figure 3 shows

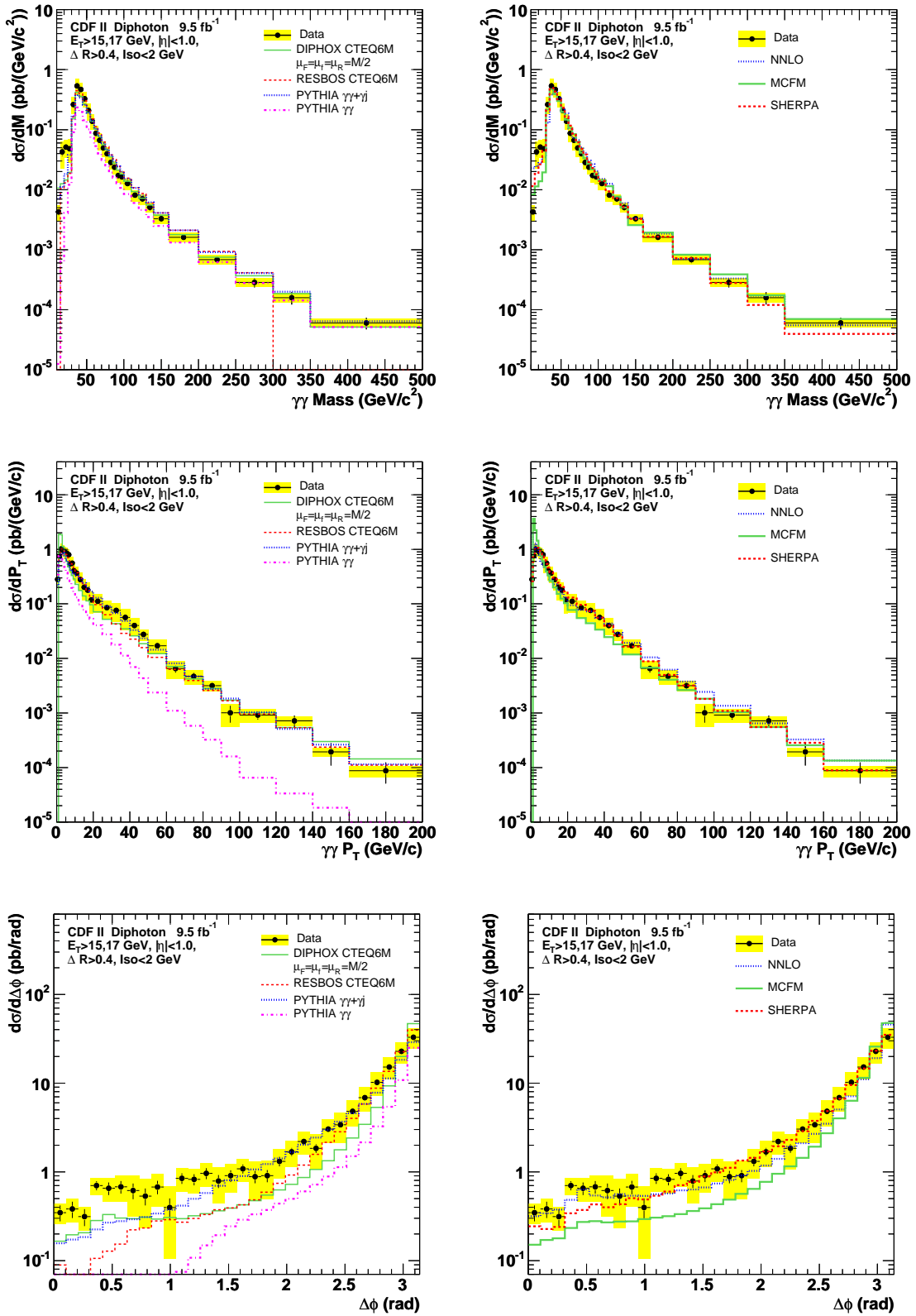


Figure 1. Measured differential cross sections as functions of the diphoton mass (top) and transverse momentum (middle), and of the azimuthal difference between the photon directions (bottom), compared with six theoretical predictions discussed in the text. The shaded area around the data points indicates the total systematic uncertainty of the measurement.

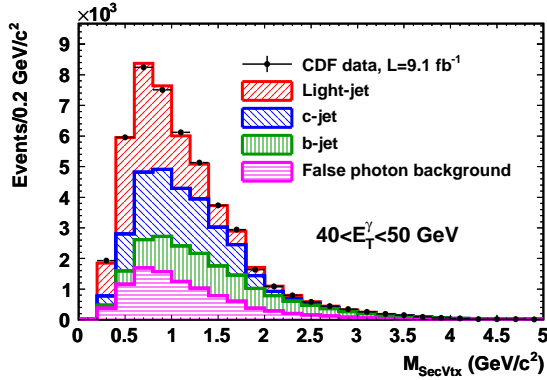


Figure 3. Distribution of the secondary-vertex mass of tagged jets for photon candidates with $40 < E_T^\gamma < 50$ GeV. The points are data, and the stacked, shaded histograms represent the estimated contributions from the fit of the b -, c -, and light-quark jets and false photon background.

the result of the fit for E_T^γ between 40 and 50 GeV, as an example.

The differential cross section is obtained from the histogram of the estimated signal yield as a function of photon E_T . The average cross section in a bin is determined by dividing the yield by the product of the trigger efficiency, the selection efficiency and acceptance, the integrated luminosity, and the bin size. The experimental results are compared with four theoretical calculations: (i) the fixed NLO calculations, including direct photon production subprocesses and subprocesses where the photon is emitted from parton fragmentation, both at $O(\alpha\alpha_s^2)$, (ii) the k_T -factorization calculations, including $O(\alpha\alpha_s^2)$ off-shell amplitudes of gluon-gluon fusion and quark-(anti)quark interaction subprocesses, and the k_T -dependent (i.e., unintegrated) parton distributions, where k_T denotes the transverse momentum of the parton, (iii) the SHERPA calculations, including all the tree-level matrix-element diagrams with one photon and up to three jets, with at least one b jet or c jet in the explored kinematic region, (iv) the PYTHIA calculations, including the $2 \rightarrow 2$ matrix-element subprocesses $gb \rightarrow \gamma b$ and $q\bar{q} \rightarrow \gamma g$ with $g \rightarrow b\bar{b}$ and $g \rightarrow c\bar{c}$ splittings in the parton shower. Previous studies [5] showed that the contribution of gluon splitting to heavy flavor has to be approximately doubled over expectations from the leading-order PYTHIA generator to reproduce the data. Hence, we also show predictions that include a double gluon-splitting rate to heavy flavors.

Figure 4 shows the comparisons between the observed and predicted distributions in photon E_T . The NLO pQCD predictions agree with data at low E_T^γ but fail to describe data for $E_T^\gamma > 70$ GeV for the bottom-jet cross section. The same trend is observed in the charm-jet cross section even though the experimental uncertainty is larger. For large E_T^γ , the dominant production process yielding a photon and a heavy quark involves a final-state gluon splitting into a heavy-flavor pair. This process is present only at leading order in the NLO calculation. The SHERPA prediction allows up to three partons in the final state, through the inclusion of additional tree-level amplitudes. The additional amplitudes also serve as a source of heavy-flavor pairs (through gluon splitting), which is important for the high E_T^γ range. The k_T -factorization and SHERPA predictions are in reasonable agreement with the measured cross sections. The PYTHIA predictions disagree with the data both in rate and in shape. Scaling the PYTHIA prediction and doubling the rate for $g \rightarrow b\bar{b}$ or $g \rightarrow c\bar{c}$ leads to an improved agreement with the data.

4 Conclusions

In conclusion, we measure the differential cross sections for diphoton production and for inclusive production of a photon in association with a heavy flavor quark. The observed cross sections are compared with a wide variety of theoretical predictions. The results are important for high precision measurements of the recently discovered Higgs bosonlike particle and searches for new phenomena in diphoton final states and in final states involving the production of photons in association with heavy-flavor quarks.

References

- [1] T. Aaltonen *et al.* (CDF Collaboration), Phys. Rev. Lett. **110**, 101801 (2013).
- [2] T. Aaltonen *et al.* (CDF Collaboration), Phys. Rev. Lett. **111**, 042003 (2013).
- [3] D. Acosta *et al.* (CDF Collaboration), Phys. Rev. D **71**, 052003 (2005).
- [4] T. Aaltonen *et al.* (CDF Collaboration), Phys. Rev. D **84**, 052006 (2011).
- [5] B. Abbott *et al.* (D0 Collaboration), Phys. Lett. B **487**, 264 (2000); D. Acosta *et al.* (CDF Collaboration), Phys. Rev. D **71**, 092001 (2005); T. Aaltonen *et al.* (CDF Collaboration), Phys. Rev. D **78**, 072005 (2008).

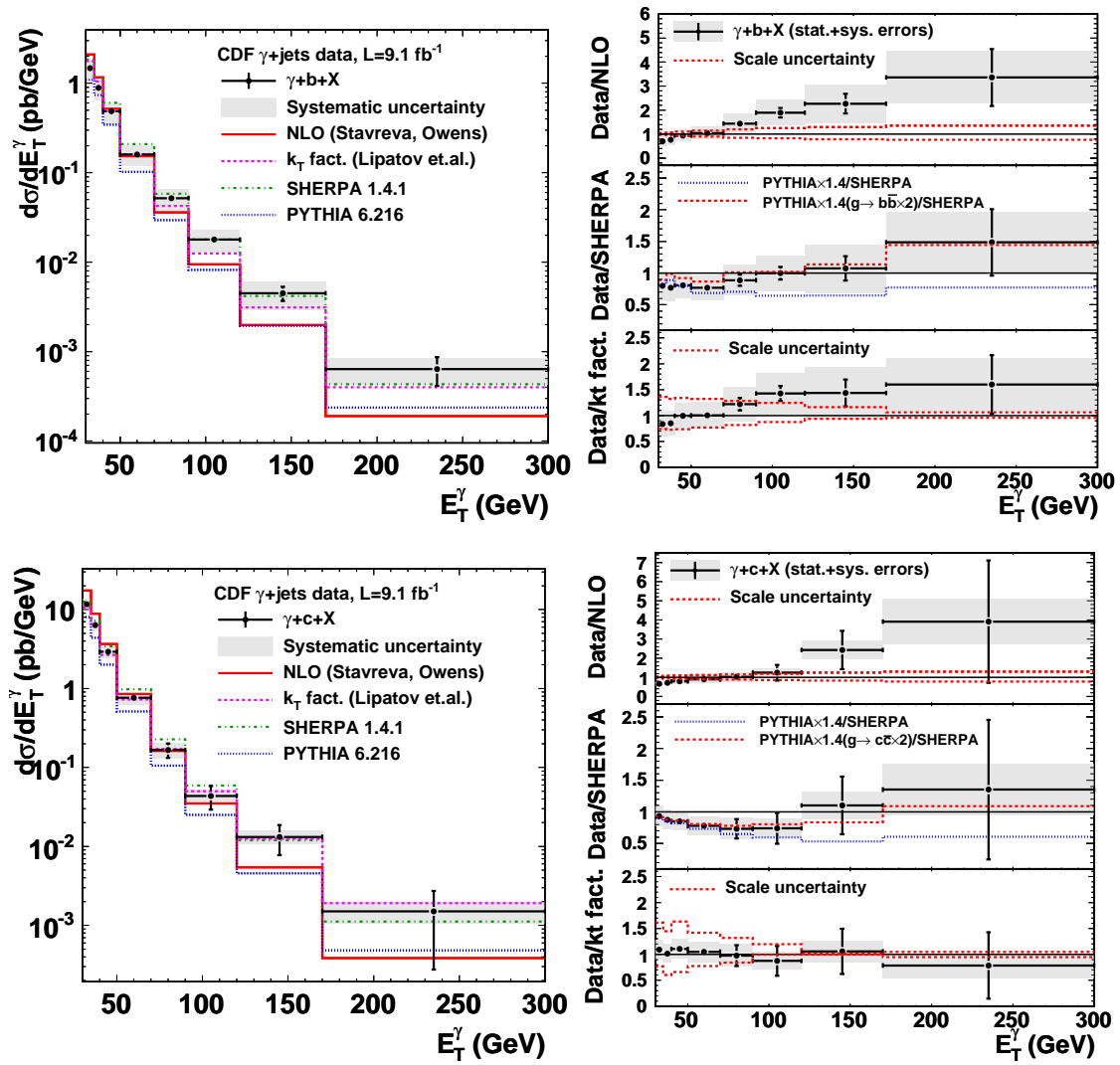


Figure 4. The measured differential cross sections compared with theoretical predictions. The left panels show the absolute comparisons and the right panels show the ratios of the data over the theoretical predictions. The PYTHIA predictions are scaled by 1.4 in the ratio distributions. The comparisons are shown for $\gamma + b + X$ (top) and $\gamma + c + X$ (bottom) processes. The shaded area around the data points indicates the total systematic uncertainty of the measurement. The scale uncertainties are shown for the NLO and the k_T -factorization predictions.